ACS OMEGA

Open Access

http://pubs.acs.org/journal/acsodf

Article

Performance and Mechanism of the Modified Group Regulated the MIL-101(Fe) Type Fenton-like Catalysts

Wei Guo, Ping Shi, Meiling Feng, and Shixiong Li*

Cite This: *ACS Omega* 2024, 9, 32864−32872

Read Online

ACCESS | Metrics & More | Article Recommendations | Supporting Information

ABSTRACT: In order to avoid the disadvantages of the Fenton process in wastewater treatment and reduce the cost of wastewater treatment, a series of MIL-101(Fe)-X (X = −OH, $-NH_2$, $-NO_2$, −H) solid Fenton catalysts were successfully prepared. The performance of these Fenton-like catalysts was studied with the Fenton experiment as a reference and methylene blue (MB) as an organic pollutant. The effects of the H_2O_2 concentration, catalyst dosage, and reaction pH on catalytic performance were systematically studied. The research had shown that the optimal concentration of H_2O_2 for catalytic reactions was 0.10 mmol/L and the pH was 3. At this point, their catalytic degradation MB performance was superior to the Fenton reaction and photocatalytic reaction. When the H_2O_2 participated in the reaction, the performance of MIL-101(Fe)-X (X = −OH, $-NH_2$, $-NO_2$, −H) in catalyzing the degradation of MB followed the rule of −OH > $-NH_2$ > $-NO_2$ > −H. This was due to the synergistic effect of Fenton-like catalysis and photocatalytic degradation in the catalytic degradation of MB. In addition, the electron paramagnetic resonance and electrospray ionization mass spectrometry showed that the hydroxyl radical (·OH) generated during the catalytic process first underwent a redox reaction with the highly electronegative functional groups in the MB molecule, and finally oxidized it to CO_2 and H_2O. This study successfully prepared commercially applicable Fenton-like catalysts and explored their optimal reaction conditions. This provides a technical reference for wastewater treatment.

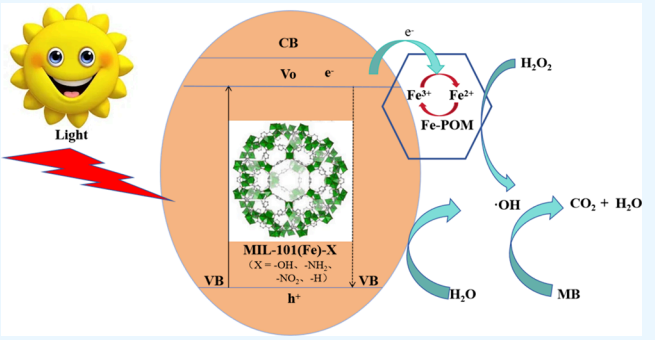

1. INTRODUCTION

Currently, environmental pollution and energy shortages restrict social development. Wastewater treatment and resource reuse are important components of implementing the concept of ecological civilization.[1] With the rapid growth of industry in our country, the amount of wastewater discharge is also increasing day by day. Energy conservation and consumption reduction, deep treatment and reuse, and standard discharge of wastewater in the wastewater treatment process have always been the focus and hotspot of people's attention. At present, the main treatment methods for industrial wastewater include adsorption method, sedimentation method, membrane separation method, electrochemical method, catalytic oxidation method, and activated sludge method.[2−4] The Fenton catalytic oxidation technology has a long history, with the advantages of low cost, fast reaction, and strong oxidation ability.[5] It can efficiently catalyze the degradation of pollutants in wastewater. However, the traditional Fenton process produces heavy metal Fe^{3+}, leading to secondary pollution of wastewater. Therefore, by the development of efficient solid-state Fenton-like catalysts,[6] the problem of secondary wastewater pollution caused by Fe^{3+} can be avoided.

Metal−organic frameworks (MOFs) are a type of material with micropores and framework structures composed of organic ligands and metal ions through coordination bonds.[7] Compared with traditional porous materials, MOFs have a higher specific surface area,[8] larger porosity,[9] and diverse and adjustable structures.[10] They are widely used in catalysis,[11−16] sensing,[17] adsorption,[18−20] and other fields.[21−27] MIL-101(Fe) and its derivatives are novel porous materials in MOFs.[13,28−30] They are constructed through organic ligands such as Fe(III) and terephthalic acid and have advantages such as large specific surface area, high porosity, and good thermal and chemical stability. They have been studied in the removal of organic pollutants through adsorption, photocatalytic degradation,[13] and Fenton-like catalysis.[31] The study also found that MIL-101(Fe) constructed with modified groups −OH and $-NH_2$ exhibited excellent photocatalytic performance.[13,32−35] In

Received: April 15, 2024
Revised: July 3, 2024
Accepted: July 5, 2024
Published: July 18, 2024

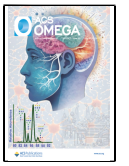

addition, MOFs have a high specific surface area and a controllable chemical environment, which can provide more active sites and optimized reaction conditions, thereby enhancing the catalytic performance of the Fenton catalysts. Moreover, MOF-based Fenton-like catalysts can overcome the problems of traditional Fenton catalysts being susceptible to neutralization and deactivation during the biodegradation process, providing new ideas and solutions for solving the limitations of traditional catalysts.

In this article, a series of MIL-101(Fe)-X (X = −OH, $-NH_2$, $-NO_2$, −H) solid-state Fenton catalysts were successfully prepared. Their structures were characterized by Fourier transform infrared spectroscopy (IR), powder X-ray diffraction (XRD), and N_2 adsorption/desorption isotherms. The performance of these Fenton-like catalysts was studied by the Fenton experiment as a reference and methyl blue (MB) as an organic pollutant. The effects of the H_2O_2 concentration, catalyst dosage, and reaction pH on the Fenton-like performance were systematically studied. The research results indicate that modified groups can effectively regulate the performance of MOF solid-state Fenton catalysts. This is due to the synergistic effect of Fenton-like catalysis and photocatalytic degradation in the catalytic degradation of MB.

2. EXPERIMENTAL SECTION

2.1. Chemical Reagents and Instruments. All solvents and chemicals were commercial reagents and used without further purification. The $FeCl_3·6H_2O$, terephthalic acid, 2-hydroxyterephthalic acid, 2-aminoterephthalic acid, 2-nitroterephthalic acid, acetic acid, *N*,*N*-dimethylformamide (DMF), anhydrous methanol, and methylene blue (MB) were purchased from Saen Chemical Technology (Shanghai) Co., Ltd. The IR spectra were measured from KBr pellets on a Nicolet 5DX FT-IR spectrometer. The X-ray phase analysis was carried out using Rigaku's D/max 2500 X-ray diffractometer with Cu Kα radiation (λ = 0.15604 nm); the tube voltage was 40 kV, the tube current was 150 mA, a graphite monochromator was used, and 2θ was 5° to 50°. The surface area was determined using the BET technique; the apparatus (AUTO CHEMII 2920) was employed to determine the surface area by using N_2 as the probe gas. The X-ray photoelectron spectroscopy (XPS) was performed on a Kratos Axis Ultra DLD system with a base pressure of 10^{-9} Torr. The zeta potentials of nanomaterials were measured by a Zetasizer (ZEN 3600, Malvern, UK). The scanning electron microscopy (SEM) was performed by using a Hitachi S-4800 instrument under the following conditions: Mag.: 1 KX, Signal A: VPSE, and EHT: 20 kV. The UV−vis absorption spectra were measured by a UV-2700 instrument from Shimadzu of Japan. The concentration of MB in solution was measured with a UV−vis 2550 in 664 nm wavelength.

2.2. Synthesis of MIL-101(Fe)-X. *2.2.1. Synthesis of MIL-101(Fe).* The MIL-101(Fe) was synthesized according to the method described in the reference.[13] Weighed $FeCl_3·6H_2O$ (0.6758 g, 2.5 mmol) and terephthalic acid (0.2075 g, 1.25 mmol) were weighed into a beaker containing 90 mL of DMF. Dissolved the mixed solution in ultrasound. Then, 3.6 mL of acetic acid was added to the mixed solution. Finally, the mixed solution was transferred to the inner liner of a 250 mL hydrothermal synthesis reactor. Heated in a blast drying oven at 110 °C for 24 h and cooled to room temperature to collect a light yellow powder. Washed the collected powder three times with DMF and methanol, and dried it in a vacuum drying oven at 80 °C for 16 h to obtain MIL-101(Fe) powder. The yield is about 92% (based on terephthalic acid).

2.2.2. Synthesis of MIL-101(Fe)−NO_2. The synthesis method was similar to that for MIL-101(Fe), except that the organic ligand was 2-nitroterephthalic acid. The specific synthesis is as follows: Weighed $FeCl_3·6H_2O$ (0.6758 g, 2.5 mmol) and terephthalic acid (0.2639 g, 1.25 mmol) into a beaker containing 90 mL of DMF. Dissolved the mixed solution in ultrasound. Then, 3.6 mL of acetic acid was added to the mixed solution. Finally, the mixed solution was transferred to the inner liner of a 250 mL hydrothermal synthesis reactor. Heated in a blast drying oven at 110 °C for 24 h. The yellow MIL-101(Fe)−NO_2 was obtained after cooling to room temperature. The collected powder was washed three times with DMF and methanol and dried in a vacuum drying oven at 80 °C for 16 h to obtain MIL-101(Fe)−NO_2 powder. Yield was about 95% (based on 2-nitroterephthalic acid).

2.2.3. Synthesis of MIL-101(Fe)−NH_2. The synthesis method was similar to that of MIL-101(Fe), except that the organic ligand was 2-aminoterephthalic acid. The specific synthesis is as follows: Weighed $FeCl_3·6H_2O$ (0.6758 g, 2.5 mmol) and terephthalic acid (0.2264 g, 1.25 mmol) into a beaker containing 90 mL of DMF. Dissolved the mixed solution in ultrasound. Then, 3.6 mL of acetic acid was added to the mixed solution. Finally, the mixed solution was transferred to the inner liner of a 250 mL hydrothermal synthesis reactor. Heated in a blast drying oven at 110 °C for 24 h. The yellow MIL-101(Fe)−NH_2 was obtained after cooling to room temperature. The collected powder was washed three times with DMF and methanol and dried in a vacuum drying oven at 80 °C for 16 h to obtain gray MIL-101(Fe)−NH_2 powder. Yield was about 92% (based on 2-aminoterephthalic acid).

2.2.4. Synthesis of MIL-101(Fe)−OH. The MIL101(Fe)−OH was synthesized by a ligand exchange method. Weighed 0.1000 g of MIL-101(Fe) and 0.1820 g of 2-hydroxyterephthalic acid in 90 mL of DMF. The suspension solution was evenly dispersed by an ultrasonic cleaning machine. The suspension was sealed in a stainless steel container with a 250 mL poly(tetrafluoroethylene) inner liner and heated in a 110 °C oven for 24 h. Cooled to room temperature when the reaction was completed. The brick red solid powder was obtained. The collected powder was washed three times with DMF and methanol and dried in a vacuum drying oven at 80 °C for 16 h to obtain MIL-101(Fe)−OH powder. The yield was about 86% (based on Fe).

2.3. Fenton and Fenton-like Experiments. At room temperature, the performance of MIL-101(Fe)-X (X = −OH, $-NH_2$, $-NO_2$, −H) Fenton catalysts was studied by the Fenton experiment as a reference and MB (C_0 = 10 mg/L, dosage 50 mL) as an organic pollutant. The effects of H_2O_2 concentration (0.05−0.20 mmol), catalyst dosage (1−9 mg), and reaction pH (1−7) on the Fenton-like performance were systematically studied. The catalytic reaction was carried out by a 250 mL circular glass reactor with a circulating water device under 300 W xenon lamp irradiation. (The light radiation intensity was about 15 W/m^2.) After reacting for 5, 10, 15, 20, and 25 min at room temperature, analyzed the concentration of MB in the solution by a spectrophotometer. Evaluated the catalytic performance by observing the changes in MB concentration before and after the reaction. The degradation rate was calculated as follows:

https://doi.org/10.1021/acsomega.4c03616
ACS Omega 2024, 9, 32864−32872

$$\eta = \frac{C_0 - C_t}{C_t} \times 100\% \quad (1)$$

Among them, η was the degradation rate (%), C_0 was the initial concentration of MB (mg/L), and C_t was the concentration of MB (mg/L) at the time of t.

2.4. Photocatalytic Degradation Experiment. In order to facilitate the comparison of catalytic performance of the Fenton-like reactions, independent photocatalytic degradation experiments of MB were conducted. The experiment of photocatalytic degradation of MB by MIL-101(Fe)-X (X = −OH, $-NH_2$, $-NO_2$, −H) was carried out under 300 W xenon lamp irradiation. The reaction conditions of the experiment are as follows: the concentration of MB was 10 mg/L, the dosage was 50 mL; the catalyst dosage was 1−9 mg; the reaction pH was 1−7; and the irradiation intensity of the lamp was 15 W/m^2. Eq 1 was also used to calculate the degradation rate of MB.

2.5. Adsorption Experiment. Due to the large specific surface area and abundant active sites of MIL-101(Fe)-X (X = −OH, $-NH_2$, $-NO_2$, −H), as well as their ability to absorb MB. In order to better illustrate the performance of Fenton-like and photocatalytic degradation of MB, the adsorption experiments were independently conducted. The adsorption experiment is similar to the Fenton-like reaction. It is just that there was no illumination during the adsorption experiment. Similarly, the eq 1 was used to calculate the removal rate of MB.

3. RESULTS AND DISCUSSION

3.1. Structure of MIL-101(Fe)-X. Herein, a series of MIL-101(Fe)-X (X = −OH, $-NH_2$, $-NO_2$, −H) solid-state Fenton catalysts were successfully prepared by Fe(III) as metal ions and terephthalic acid and its derivatives as organic ligands. It was very interesting that MIL-101(Fe) generated by the reaction of Fe(III) with colorless terephthalic acid was light yellow (Figure 1a); MIL-101(Fe)−NO_2 generated by the reaction of Fe(III) with colorless 2-nitroterephthalic acid was yellow (Figure 1b); MIL-101(Fe)−NH_2 generated by the reaction of Fe(III) with light yellow 2-aminoterephthalic acid was gray (Figure 1c); MIL-101(Fe)−OH generated by the reaction of Fe(III) with colorless 2-hydroxyterephthalic acid was brick red (Figure 1d). The SEM observation found that the particle diameter of powdered MIL-101(Fe)-X (X = −OH, $-NH_2$, $-NO_2$, −H) is about 500 nm (Figure 2). The physical and chemical properties, including structure, functional groups, elemental composition, valence states, and morphology, were studied by IR, XPS, XRD, and N_2 adsorption/desorption isotherms.

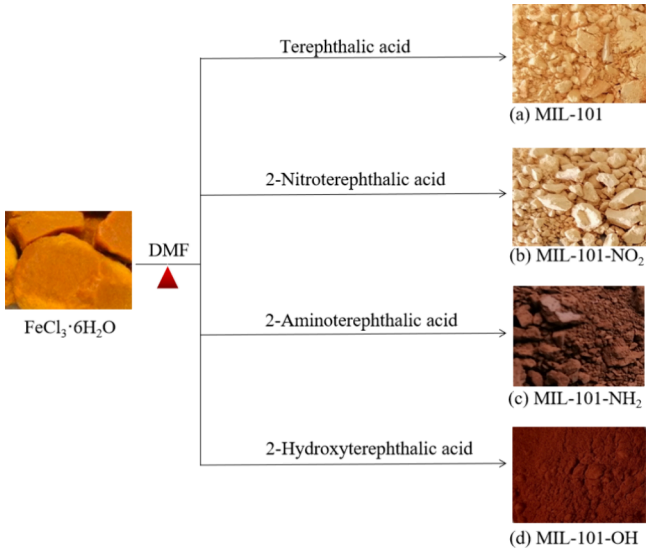

Figure 1. Synthesis and color of MIL-101(Fe)-X: (a) MIL-101; (b) MIL-101-NO_2; (c) MIL-101-NH_2; (d) MIL-101-OH.

3.1.1. IR. The IR of materials can effectively determine which functional groups exist in their structures. The IR of MIL-101(Fe) (Figure S1a) indicated a stretching vibration absorption peak of ν(C═O) at 1658 cm^{-1}, and a stretching vibration absorption peak of ν(C−O) at 1397 cm^{-1}. When different functional groups (−OH, $-NH_2$, and $-NO_2$) were introduced into MIL-101(Fe), the IR absorption peaks of these functional groups were also observed. For example, in MIL-101(Fe)−NO_2 (Figure S1b), there was a stretching vibration absorption peak of ν(CN) at 1121 cm^{-1}, an antisymmetric stretching vibration absorption peak of $-NO_2$ at 1540 cm^{-1}, and a symmetric stretching vibration absorption peak of $-NO_2$ at 1390 cm^{-1}. These absorption peaks are within the range reported in the literature;[36] In MIL-101(Fe)−NH_2 (Figure S1c), there was a ν(C−N) stretching vibration absorption peak at point 1127 cm^{-1}, a ν(N−H) stretching vibration absorption peak at point 3462 cm^{-1}, and a ν(N−H) out of plane bending absorption peak at point 767 cm^{-1}; In MIL-101 (Fe)−OH (Figure S1d), there was a stretching vibration absorption peak of ν(O−H) at 3436 cm^{-1}, an in-plane bending vibration absorption peak of ν(O−H) at 1376 cm^{-1}, an out of plane bending vibration absorption peak of ν(O−H) at 694 cm^{-1}, and a stretching vibration absorption peak of ν(C═O) at 1245 cm^{-1}.

3.1.2. XRD. X-ray powder diffraction (XRD) can be used to analyze the purity of materials and determine their structure. From the XRD pattern of MIL-101(Fe)-X (X = −OH, $-NH_2$, $-NO_2$, −H) (Figure 3), it can be seen that they have a higher crystallinity between 5° and 20°. There are obvious sharp diffraction peaks at 8.39°, 9.04°, 9.85°, and 16.42° (JCPDS No. 24-0072). The crystal planes corresponding to the peaks described above show that their central ions are Fe(III). Their diffraction peaks have high intensity, indicating the high purity of the materials. In addition, the XRD diffraction patterns of the synthesized MIL-101(Fe)-X (X = −OH, $-NH_2$, $-NO_2$, −H) were consistent with the theoretical simulation of MIL-101(Fe). This indicated that MIL-101(Fe)-X (X = −OH, $-NH_2$, $-NO_2$, and −H) had been successfully synthesized.

3.1.3. XPS. The elemental composition and valence state of MIL-101(Fe)-X (X = −OH, $-NH_2$, $-NO_2$, and −H) were characterized and analyzed by XPS. The XPS of MIL-101(Fe) (Figure S2) showed that it was mainly composed of C, O, and Fe elements (Figure S2a). The characteristic orbital peaks of C(1s) and O(1s) were found at 284.8 eV (Figure S2b) and 531.6 eV (Figure S2c), respectively. Since there was no satellite (Figure S2d) peak between Fe($2P_{1/2}$) and Fe($2P_{3/2}$), the central ion of MIL-101(Fe) was Fe(III). The XPS of MIL-101(Fe)−NO_2 (Figure S3) showed that it was mainly composed of C, N, O, and Fe elements (Figure S3a). The characteristic orbital peaks of C(1s), N(1s), and O(1s) were found at 284.8 eV (Figure S3b), 405.5 eV (Figure S3c), and 531.5 eV (Figure S3d), respectively. The MIL101(Fe)−NO_2 was the same as MIL101(Fe), its central ion was also Fe(III) (Figure S3e). The XPS of MIL101(Fe)−NH_2 (Figure S4) also

https://doi.org/10.1021/acsomega.4c03616
ACS Omega 2024, 9, 32864−32872

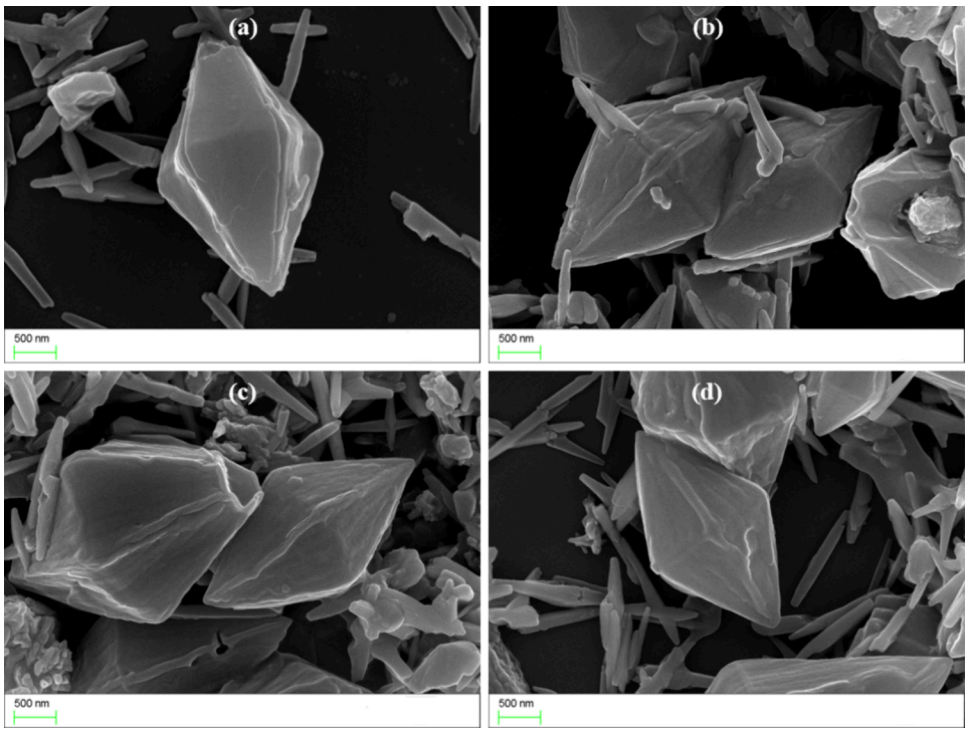

Figure 2. SEM: (a) MIL-101; (b) MIL-101-NO_2; (c) MIL-101-NH_2; (d) MIL-101-OH.

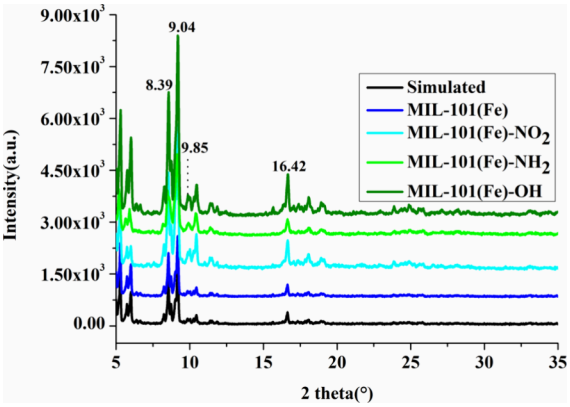

Figure 3. XRD of MIL-101(Fe)-X (X = −OH, $-NH_2$, $-NO_2$, −H).

showed that it was composed of C, N, and O elements, and the central ion is Fe(III). In addition, the XPS of MIL101(Fe)−OH (Figure S5) also showed that it was composed of C and O elements, and the central ion was Fe(III).

3.1.4. N_2 Adsorption/Desorption Isotherms. The characterization of N_2 adsorption/desorption isotherms for MIL-101(Fe)-X (X = −OH, $-NH_2$, $-NO_2$, −H) indicated that they were typical Type I adsorption isotherms (Figure S6 and Table S1). It can be clearly seen from Figure S6 that the MIL-101(Fe) has a very large specific surface area, which can reach up to 3153 $m^2\ g^{-1}$. When different functional groups were introduced into the structure of MIL-101(Fe), their specific surface area underwent a significant change. Among them, the specific surface areas of MIL-101(Fe)−NO_2, MIL-101(Fe)−NH_2, and MIL-101(Fe)−OH were 1880, 2010, and 2275 $m^2\ g^{-1}$, respectively. Due to the introduction of different functional groups, their surface areas in similar structures are all smaller than those of MIL-101(Fe). However, their adsorption type (Type I) and specific surface area are consistent with those reported in the literature.[13,28−30]

3.1.5. UV−Visible Absorption Spectrum. The UV−visible absorption spectroscopy can be used to analyze the light absorption behavior of photocatalysts and calculate their bandgaps. The UV absorption spectrum of MIL-101(Fe)-X (X = −OH, $-NH_2$, $-NO_2$, −H) (Figure 4) shows that they

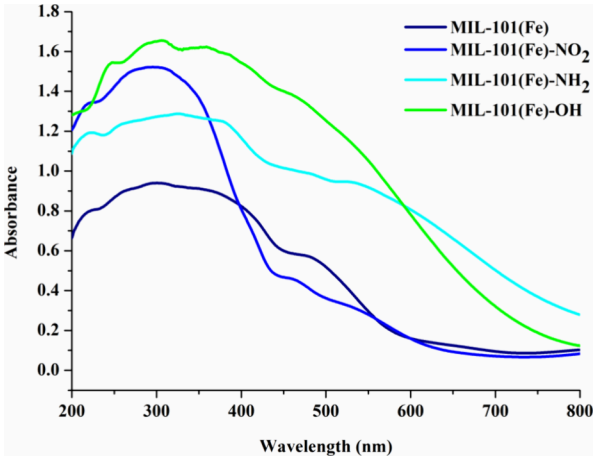

Figure 4. UV−visible absorption spectrum of MIL-101(Fe)-X (X = −OH, $-NH_2$, $-NO_2$, −H).

have strong light absorption behavior at 200−800 nm. Especially after the $-NH_2$ and −OH functional groups with extra lone electrons are introduced into MIL-101(Fe), they show stronger light absorption. This is because when there is $-NH_2$ or −OH on the organic ligand, the extra lone electrons on their functional groups can form p-π conjugation with the aromatic ring in the ligand. Thereby affecting their light absorption through the effect of LMCT. In addition, it can be

https://doi.org/10.1021/acsomega.4c03616
ACS Omega 2024, 9, 32864−32872

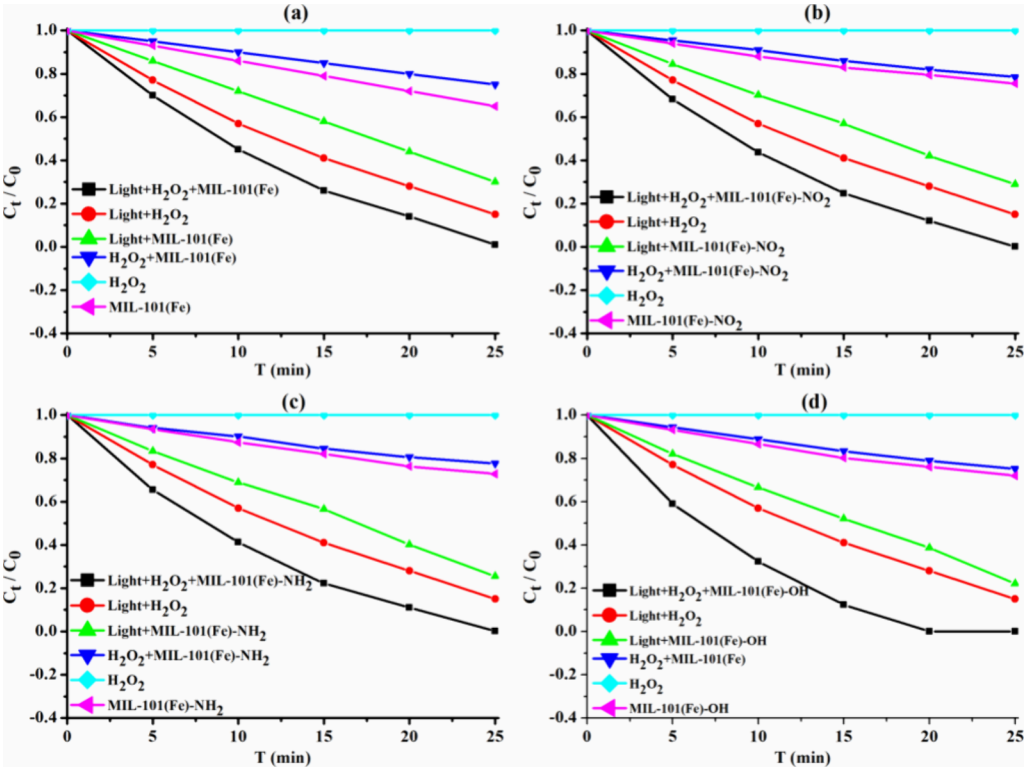

Figure 5. Activity control experiment: (a) MIL-101(Fe); (b) MIL-101(Fe)−NO_2; (c) MIL-101(Fe)−NH_2; (d) MIL-101(Fe)−OH.

found from Figure 4 that in MIL-101(Fe)-X (X = −OH, $-NH_2$, $-NO_2$, −H), their light absorption behavior follows the rules of −OH > $-NH_2$ > $-NO_2$ > −H. When using the formula $E_g = 1240/\lambda g$, it can be roughly calculated that their bandgap widths (E_g) are 2.53, 2.19, 2.02, and 1.64 eV, respectively. Therefore, MIL-101(Fe)-X (X = −OH, $-NH_2$, $-NO_2$, −H) has strong light absorption behavior at 200−800 nm. The impact of their photocatalytic pollutant degradation performance needs to be considered when exploring their Fenton-like catalytic properties.

3.2. Catalytic Performance. *3.2.1. Activity Control Experiment (Light and Fenton-like).* A control experiment was conducted on the activity of the Fenton-like reaction in the degradation of MB at room temperature (The catalyst dosage was 5.0 mg, the concentration of H_2O_2 was 0.10 mmol, and the solution pH was 3.) They mainly included Fenton-like reactions, Fenton reactions, adsorption, and photocatalytic reactions of MIL-101(Fe)-X (X = −OH, $-NH_2$, $-NO_2$, and −H). The experimental results (Figure 5) indicate that after 25 min of reaction in these systems, the degradation rate of MB follows the order of Fenton-like reaction > Fenton reaction > photocatalytic reaction > adsorption reaction > MB + H_2O_2. Among them, in the Fenton-like reaction of MIL-101(Fe) (Figure 5a), the removal rates of MB could reach 99.0% after 25 min. However, the degradation rates of MB by Fenton catalytic reaction, photocatalytic reaction, and adsorption reaction were 85.1, 70.4, and 35.1%, respectively. In the Fenton-like reaction of MIL-101(Fe)−NO_2 (Figure 5b), the removal rates of MB by the Fenton-like catalytic reaction, photocatalytic reaction, and adsorption reaction were 100, 61.1, and 24.5%, respectively; In the Fenton-like reaction of MIL-101(Fe)−NH_2 (Figure 5c), the removal rates of MB by the Fenton-like catalytic reaction, photocatalytic reaction, and adsorption reaction were 100, 74.5, and 27.2%, respectively. In the Fenton-like reaction of MIL-101(Fe)−OH (Figure 5d), some experiments were completed after 20 min. The removal rates of MB by Fenton-like catalytic reactions, Fenton catalytic reactions, photocatalytic reactions, and adsorption reactions were 100, 72.0, 61.3, and 23.9%, respectively.

Based on the comprehensive analysis of the removal rates of the above reactions, it can be found that due to the large specific surface area[13] and numerous adsorption sites of MIL-101(Fe)-X (X = −OH, $-NH_2$, $-NO_2$, −H), they can adsorb a certain amount of MB; The MIL-101(Fe)-X also belongs to photocatalysts,[13] which have good performance in degrading MB. Therefore, in the MIL-101(Fe)-X Fenton-like catalytic reaction process, their performance in degrading MB follows the rule of −OH > $-NH_2$ > $-NO_2$ > −H. This is attributed to the synergistic effect of Fenton-like catalysis and photocatalytic degradation in the degradation of MB. This makes the performance of Fenton-like catalytic degradation of MB superior to the Fenton reaction and photocatalytic reaction.

3.2.2. Effect of H_2O_2 Dosage on Catalytic Performance. The effect of H_2O_2 concentration (0.05−0.20 mmol/L) on the catalytic degradation performance of MB was investigated at room temperature (The catalyst dosage was 5.0 mg, and the pH was 3). The experimental results (Figure S7) showed that the degradation rate of MB did not increase with the increase in H_2O_2 concentration after 25 min of catalytic degradation. Among them, in the catalytic reaction of MIL-101(Fe) (Figure S7a), the degradation rates of MB were 88.1, 99.0, 93.8, and 85.2%, respectively; in the catalytic reaction of MIL-101(Fe)−NO_2 (Figure S7b), the degradation rates of MB were 90.2, 100, 95.2, and 86.9%, respectively; In the catalytic reaction of MIL-101(Fe)−NH_2 (Figure S7c), the degradation rates of MB were 93.1, 100, 96.8, and 89.3%, respectively; In the catalytic reaction of MIL-101(Fe)−OH (Figure S7d), the degradation rates of MB were 99.1, 100, 100, and 91.9%, respectively. A

https://doi.org/10.1021/acsomega.4c03616
ACS Omega 2024, 9, 32864−32872

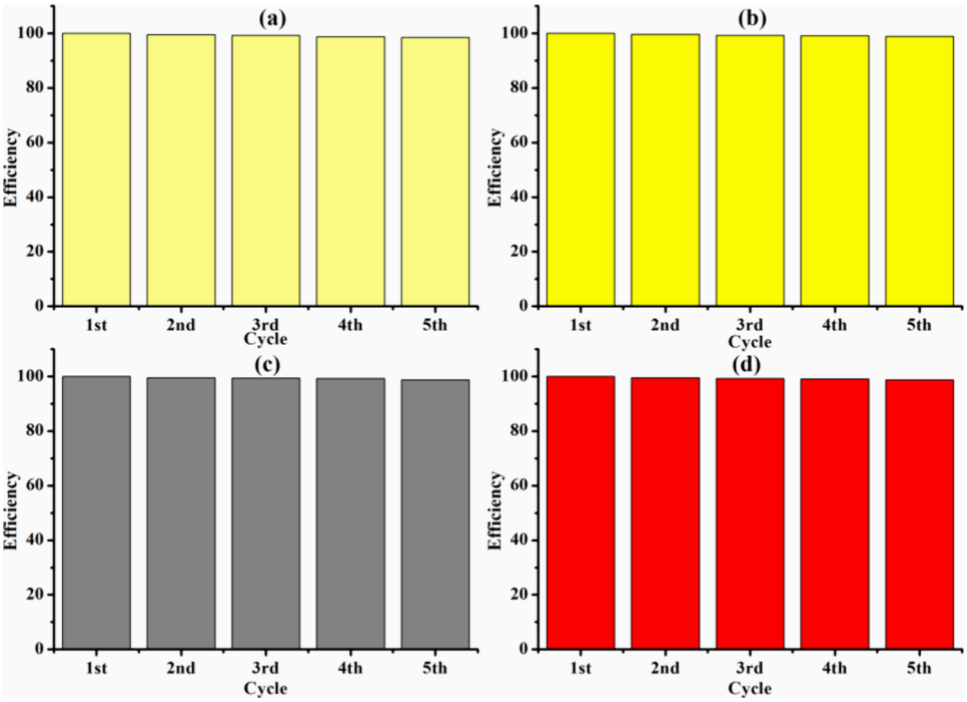

Figure 6. Cycle experiment: (a) MIL-101(Fe); (b) MIL-101(Fe)−NO_2; (c) MIL-101(Fe)−NH_2; (d) MIL-101(Fe)−OH.

comprehensive analysis of the effect of H_2O_2 concentration (0.05−0.20 mmol/L) on the catalytic degradation performance of MB, which reveals that when the H_2O_2 concentration is between 0.05 and 0.10 mmol/L, the degradation rate of MB increases with the increase of H_2O_2 concentration. When the concentration is between 0.10 and 0.20 mmol/L, the degradation rate of MB decreases with the increase of H_2O_2 concentration. This may be due to the generation of excess ·OH that does not bind to MB in a short period of time, resulting in quenching by collision between ·OH radicals or the generation of H_2O_2. The excess ·OH may also combine with H_2O_2 to produce ·H_2O with lower oxidation ability, ultimately leading to a decrease in MB degradation rate.[31] Therefore, the concentration of H_2O_2 in this Fenton-like reaction system should not be too high.[37]

3.2.3. Effect of Catalyst Dosage on Catalytic Performance. The effect of catalyst dosage (1−9 mg) on the catalytic degradation performance of MB was explored at room temperature (the H_2O_2 dosage was 0.10 mmol/L, and the pH was 3). The experimental results showed that after 25 min of catalytic degradation reaction, the degradation rate of MB did not increase rapidly with the increase in catalyst dosage (Figure S8). Among them, in the catalytic reaction of MIL-101(Fe) (Figure S8a), the degradation rates of MB were 82.7, 88.8, 99.0, 95.1, and 94.2%, respectively; In the catalytic reaction of MIL-101(Fe)−NO_2 (Figure S8b), the degradation rates of MB were 83.5, 89.7, 100, 96.0, and 95.1%, respectively; In the catalytic reaction of MIL-101(Fe)−NH_2 (Figure S8c), the degradation rates of MB were 88.9, 95.1, 100, 99.0, and 97.1%, respectively; In the catalytic reaction of MIL-101(Fe)−OH (Figure S8d), the degradation rates of MB were 99.1, 100, 100, 100, and 100%, respectively. A comprehensive analysis of the effect of catalyst dosage (1−9 mg) on the catalytic degradation performance of MB reveals that when the catalyst dosage is 1−5 mg, the degradation rate of MB increases with the increase of catalyst dosage. When the catalyst dosage is between 5 and 9 mg, the degradation rate of MB decreases with the increase of catalyst dosage, but the reduction is not significant. This may be due to the increase in ·OH concentration generated in the system when the dosage is below 5 mg, which leads to an increase in the degradation rate of MB. Because when the catalyst dosage is 5 mg, the concentration of ·OH generated reaches saturation. When the catalyst dosage exceeds 5 mg, the concentration of ·OH generated at a certain H_2O_2 concentration cannot be further increased. Moreover, due to the masking effect of the material on light, the dosage exceeding 5 mg will lead to a decrease in light intensity, resulting in a decrease in degradation efficiency.[38]

3.2.4. Effect of Initial pH of Solution on Catalytic Performance. The effect of pH (1−7) on the catalytic degradation performance of MB was explored under conditions of room temperature (The H_2O_2 dosage was 0.10 mmol/L, and the catalyst dosage was 5 mg). The traditional Fenton reaction requires a lower pH.[39] However, after 25 min of catalytic degradation of MB by MIL-101(Fe)-X (X = −OH, −NH_2, −NO_2, −H), the degradation rate of MB did not increase with the decrease of pH (Figure S9). Among them, in the catalytic reaction of MIL-101(Fe) (Figure S5a), the degradation rates of MB were 94.1, 99.0, 85.9, and 79.0%, respectively. In the catalytic reaction of MIL-101(Fe)−NO_2 (Figure S9b), the degradation rates of MB were 97.2, 100, 83.7, and 71.1%, respectively. In the catalytic reaction of MIL-101(Fe)−NH_2 (Figure S9c), the degradation rates of MB were 98.1, 100, 92.2, and 84.5%, respectively; In the catalytic reaction of MIL-101(Fe)−OH (Figure S9d), the degradation rates of MB were 100, 100, 100, and 87.9%, respectively. A comprehensive analysis of the effect of pH (1−7) on the catalytic degradation performance of MB reveals that the catalytic degradation performance of MB is best at pH = 3. It is superior to the performance at pH 1, 5, and 7. Usually, the lower pH is beneficial for prolonging the recombination of

https://doi.org/10.1021/acsomega.4c03616
ACS Omega 2024, 9, 32864−32872

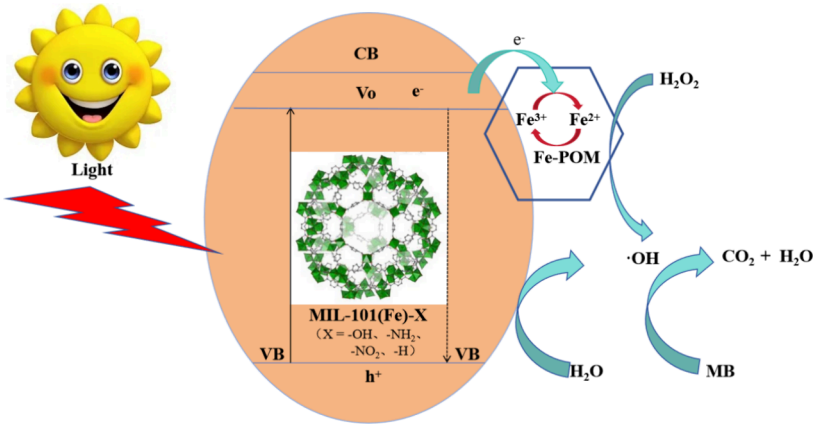

Figure 7. Mechanism of catalytic degradation of MB by MIL-101(Fe)-X (X = −OH, $-NH_2$, $-NO_2$, −H).

electrons and holes generated during photocatalytic degradation, thereby improving catalytic efficiency.[13] The zeta potential (Table S2) of MIL-101(Fe)-X (X = −OH, $-NH_2$, $-NO_2$, −H) also illustrates this point. However, based on the same catalyst dosage and pH conditions, MIL-101(Fe)-X (X = −OH, $-NH_2$, $-NO_2$, −H) has better catalytic degradation performance of MB in the presence of H_2O_2 than performance of MIL-101(Fe)[40−42] in photocatalytic degradation of MB.

3.3. Cycle Experiment. The catalyzed powder catalyst was collected by a high-speed centrifuge at 11,000 rpm. Then, 0.001 mol/L HNO_3 was added to the collected powder catalyst, and ultrasonic treatment was performed for 10 min. Continued to collect the powdered catalyst by a high-speed centrifuge at 11,000 rpm. The collected catalyst was then washed three times with anhydrous methanol and deionized water, respectively. The washed solid powder was heated in a blast drying oven at 100 °C for 8 h. The collected solid catalyst was characterized by XRD. The test results (Figure S10) showed that the position of the diffraction peak of the catalyzed catalyst was consistent with the theoretical simulation of MIL-101(Fe). This shows that the structure remains unchanged after the catalytic degradation of MB by MIL-101(Fe)-X (X = −OH, $-NH_2$, $-NO_2$, and −H). In addition, the XPS (Figure S11) also shows that the valence state of iron after MIL-101(Fe)-X (X = −OH, $-NH_2$, $-NO_2$, −H) catalyzed MB is still +3.

The cycle experimental (Figure 6) results of like-Fenton catalytic degradation of MB by MIL-101(Fe)-X (X = −OH, $-NH_2$, $-NO_2$, −H) showed that after the first cycle of MIL-101(Fe), the efficiency could be maintained at 100%, even after five cycles, its catalytic degradation efficiency of MB could still be maintained at 98.5% (Figure 6a). Similarly, the efficiency of MIL-101(Fe)−NO_2 (Figure 6b), MIL-101(Fe)−NH_2 (Figure 6c), and MIL-101(Fe)−OH (Figure 6d) in the first cycle of catalysis could all be maintained at 100%. However, after five cycles of catalysis, the efficiencies of MIL-101(Fe)−NO_2, MIL-101(Fe)−NH_2, and MIL-101(Fe)−OH were 98.9, 98.8, and 98.6%, respectively. Therefore, MIL-101(Fe)-X (X = −OH, $-NH_2$, $-NO_2$, −H) Fenton-like catalyst has good structural stability and stability in the catalytic degradation of MB.

3.4. Catalytic Mechanism. In the presence of H_2O_2, there are photocatalytic degradation reactions and Fenton-like catalytic reactions in the catalytic degradation of MB by MIL-101(Fe)-X (X = −OH, $-NH_2$, $-NO_2$, and −H). The research[13] had shown that ·OH was generated during the catalytic degradation of organic pollutants by MIL-101(Fe)-X (X = −OH, $-NH_2$, $-NO_2$, −H). Therefore, MIL-101(Fe)-X (X = −OH, $-NH_2$, $-NO_2$, −H) reacted with H_2O and H_2O_2 to generate ·OH under light conditions. In addition, the electron paramagnetic resonance (EPR) also captured the presence of ·OH (Figure S12). Therefore, the ·OH played the role of an oxidant during the catalytic degradation of MB by MIL-101(Fe)-X (X = −OH, $-NH_2$, $-NO_2$, −H).

The samples were taken and characterized by electrospray ionization mass spectrometry (ESI-MS) after MIL-101(Fe)-X (X = −OH, $-NH_2$, $-NO_2$, −H) degraded MB for 15 min. There were four related molecular peaks (Figure S13) found in MB solution during the catalytic degradation process with the charge mass (m/z) ratios of 302.30, 284.12, 270.11, and 242.07, respectively. As we all know, MB is an ionic dye, which exists in the form of ions after being dissolved in water. Therefore, the m/z at 284.12 can be assigned to $[C_{16}H_{18}N_3S]^+$. The density functional theory (DFT) has proven that −C═S− and −C═N− in $[C_{16}H_{18}N_3S]^+$ have high electronegative properties,[43] and they preferentially undergo redox reactions with ·OH to generate $[C_{16}H_{22}N_3SO]$. Therefore, the m/z at 302.30 can be assigned to $[C_{16}H_{22}N_3SO]$. In $[C_{16}H_{22}N_3SO]$, the −C═S double bond has high electronegativity, and it reacts with ·OH to generate $[C_6H_9N_2SO_8]$. Therefore, the m/z at 242.07 is $[C_6H_9N_2SO_8]$. Under the oxidation of ·OH, the aromatic ring in $[C_6H_9N_2SO_8]$ is broken to generate $[C_6H_4N_2O_7S]$. Therefore, the m/z at 270.11 nm can be assigned as $[C_6H_4N_2O_7S]$. Finally, $[C_6H_4N_2O_7S]$ reacts with ·OH to ultimately generate small molecules, CO_2 and H_2O (Figure S14).

Therefore, comprehensive analysis can show that the catalytic degradation of MB by MIL-101(Fe)-X (X = −OH, $-NH_2$, $-NO_2$, −H) is the result of the synergistic effect of photocatalysis and Fenton-like catalysis (Figure 7). The ·OH first reacted with the highly electronegative functional groups in the MB molecular structure, and then oxidized and decomposed them all into CO_2 and H_2O.

4. CONCLUSION

In summary, a series of MIL-101(Fe)-X (X = −OH, $-NH_2$, $-NO_2$, −H) catalysts were synthesized by the hydrothermal synthesis method. They can effectively catalyze the degradation of MB in the presence or absence of H_2O_2. Among them, the Fenton-like catalytic performance is the best, which was superior to the Fenton reaction and photocatalytic reaction. This was because when H_2O_2 participated in catalytic

https://doi.org/10.1021/acsomega.4c03616
ACS Omega 2024, 9, 32864−32872

reactions, there were Fenton-like reactions and photocatalytic reactions. They catalyzed the reaction together and produced a large amount of ·OH, so as to rapidly catalyze the degradation of MB into CO_2 and H_2O. This study helps to avoid the drawbacks of the Fenton reaction and improve the efficiency of wastewater purification.

■ ASSOCIATED CONTENT

Supporting Information

The Supporting Information is available free of charge at https://pubs.acs.org/doi/10.1021/acsomega.4c03616.

IR, XPS, XRD, EPR, and N_2 adsorption/desorption isotherms of MIL-101(Fe)-X (X = −OH, $-NH_2$, $-NO_2$, −H); effect of H_2O_2 dosage, catalyst dosage, and pH on catalytic performance; EPR captured the presence of ·OH; ESI-MS analysis of MB degradation pathways during catalysis; possible degradation pathways of MB during catalytic reactions; specific surface area, and zeta potential of MIL-101(Fe)-X (X = −OH, $-NH_2$, $-NO_2$, −H) (PDF)

■ AUTHOR INFORMATION

Corresponding Author

Shixiong Li − *School of Mechanical and Resource Engineering, Wuzhou University, Wuzhou, Guangxi 543003, P. R. China; School of Resources Environment and Materials, Guangxi University, Nanning, Guangxi 530004, P. R. China;* orcid.org/0000-0002-6600-1749; Email: lsx1324@163.com

Authors

Wei Guo − *School of Mechanical and Resource Engineering, Wuzhou University, Wuzhou, Guangxi 543003, P. R. China; School of Resources Environment and Materials, Guangxi University, Nanning, Guangxi 530004, P. R. China*

Ping Shi − *School of Mechanical and Resource Engineering, Wuzhou University, Wuzhou, Guangxi 543003, P. R. China*

Meiling Feng − *School of Mechanical and Resource Engineering, Wuzhou University, Wuzhou, Guangxi 543003, P. R. China*

Complete contact information is available at: https://pubs.acs.org/10.1021/acsomega.4c03616

Author Contributions

W.G.: writing−original draft. P.S.: data curation. M.F.: data curation. S.L.: funding acquisition, writing—review and editing.

Notes

The authors declare no competing financial interest.

■ ACKNOWLEDGMENTS

This work was supported by the Guangxi Natural Science Foundation, China (No. 2024GXNSFAA010355); the Science and Technology Project of WuZhou (No. 202302049); and the National College Student Entrepreneurship Training Program (No. 202411354014).

■ REFERENCES

(1) Josa, I.; Garfí, M. Social life cycle assessment of microalgae-based systems for wastewater treatment and resource recovery. *J. Clean. Prod.* **2023**, *407*, No. 137121.

(2) Raj, S.; Singh, H.; Bhattacharya, J. Treatment of textile industry wastewater based on coagulation-flocculation aided sedimentation followed by adsorption: Process studies in an industrial ecology concept. *Sci. Total Environ.* **2023**, *857*, No. 159464.

(3) Kumar, A.; Thakur, A.; Panesar, P. S. A review on the industrial wastewater with the efficient treatment techniques. *Chem. Pap.* **2023**, *77* (8), 4131−4163.

(4) Li, S. X.; Feng, A. Q.; Hu, Y.; Liang, G. C.; Lu, L. F.; Lu, H. P. Two-Dimensional Copper-Based Coordination Polymer: Synthesis, Structure and Ion Effect on Adsorption of Cr(VI). *Chin. J. Inorg. Chem.* **2022**, *38* (5), 941−950.

(5) Liu, W.; Dong, Y.; Liu, J.; Zhang, L.; Lu, Y.; Lin, H. Halloysite nanotube confined interface engineering enhanced catalytic oxidation of photo-Fenton reaction for aniline aerofloat degradation: Defective heterojunction for electron transfer regulation. *Chem. Engin. J.* **2023**, *451*, No. 138666.

(6) Wang, Y.; Zhu, Q.; Xie, T.; Peng, Y.; Wang, J.; Yao, Z. Performance and mechanism of FeS_2/FeSxOy as highly effective Fenton-like catalyst for phenol degradation. *Environ. Technol.* **2023**, *44* (24), 3731−3740.

(7) Li, S. X.; Luo, P.; Wu, H. Z.; Wei, C. H.; Hu, Y.; Qiu, G. L. Strategies for improving the performance and application of MOFs photocatalysts. *ChemCatChem.* **2019**, *11* (13), 2978−2993.

(8) Pang, W.; Shao, B.; Chen, X.; Gu, Q. X.; Yang, F. J.; Li, S. X.; Huang, J. Enhancing the activity of metal-organic nanosheets for oxygen evolution reaction by substituent effects. *J. Colloid Interface Sci.* **2022**, *608*, 306−312.

(9) Cai, G.; Yan, P.; Zhang, L.; Zhou, H. C.; Jiang, H. L. Metal−organic framework-based hierarchically porous materials: synthesis and applications. *Chem. Rev.* **2021**, *121* (20), 12278−12326.

(10) Bigdeli, F.; Lollar, C. T.; Morsali, A.; Zhou, H. C. Switching in metal−organic frameworks. *Angew. Chem., Int. Ed.* **2020**, *59* (12), 4652−4669.

(11) Liao, B.; Li, S. Multifunctional Mn (II) Metal-Organic framework for photocatalytic aerobic oxidation and CH direct trifluoromethylation. *J. Catal.* **2022**, *414*, 294−301.

(12) Li, S.; Yang, S.; Liang, G.; Yan, M.; Wei, C.; Lu, Y. Regulation and photocatalytic degradation mechanism of a hydroxyl modified UiO-66 type metal organic framework. *RSC Adv.* **2023**, *13* (8), 5273−5282.

(13) Li, S. X.; Sun, S. L.; Wu, H. Z.; Wei, C. H.; Hu, Y. Effects of electron-donating groups on the photocatalytic reaction of MOFs. *Catal. Sci. Technol.* **2018**, *8* (6), 1696−1703.

(14) Liu, Y. F.; Hu, C. W.; Yang, G. P. Recent advances in polyoxometalates acid-catalyzed organic reactions. *Chin. Chem. Lett.* **2023**, *34* (5), No. 108097.

(15) Liu, Y.; Zeng, G.; Cheng, Y.; Chen, L.; Liu, Y.; Wei, Y.; Yang, G. A $H_4SiW_{12}O_{40}$-catalyzed three-component tandem reaction for the synthesis of 3, 3-disubstituted isoindolinones. *Chin, Chem, Lett.* **2024**, *35* (1), No. 108480.

(16) Zhao, J.; Dang, Z.; Muddassir, M.; Raza, S.; Zhong, A.; Wang, X.; Jin, J. A new Cd (II)-based coordination polymer for efficient photocatalytic removal of organic dyes. *Molecules* **2023**, *28* (19), 6848.

(17) Yang, G. L.; Jiang, X. L.; Xu, H.; Zhao, B. Applications of MOFs as luminescent sensors for environmental pollutants. *Small* **2021**, *17* (22), No. 2005327.

(18) Li, S.; Huang, L.; Jia, B.; Feng, X.; Cao, Y.; Chen, Y.; Bin, Y. Effect and mechanism of inorganic anions on the adsorption of Cd^{2+} on two-dimensional copper-based metal-organic framework. *Inorg. Chem. Commun.* **2024**, *159*, No. 111819.

(19) Zeng, Y.; Li, X.; Chen, Y.; Li, S. High-Efficiency Adsorption of Cr(VI) and Mn(VII) from Wastewater by a Two-Dimensional Copper-Based Metal−Organic Framework. *ACS Omega* **2023**, *8* (40), 36978−36985.

(20) Yang, S. L.; Chen, Y. H.; Yan, M. L.; Wei, C. T.; Li, S. X.; Jia, B. J. Effect of free water molecule in copper complexes on the performance of light absorption and adsorption of Cr(VI). *Chin. J. Inorg. Chem.* **2023**, *39* (11), 2160−2168.

(21) Li, S. X.; Qiang, J. W.; Liao, B. L. Structure, magnetism and oxygen reduction reaction in mixed-valent Cu (I)···Cu (II) complex supported by benzimidazole derivative. *Inorg. Chim. Acta* **2021**, *521*, No. 120356.
(22) Li, J. X.; Zhang, Y. H.; Du, Z. X.; Feng, X. One-pot solvothermal synthesis of mononuclear and oxalate-bridged binuclear nickel compounds: Structural analyses, conformation alteration and magnetic properties. *Inorg. Chim. Acta* **2022**, *530*, No. 120697.
(23) Li, S. X.; Chen, Y. H.; Yang, S. L.; Yan, M. L.; Wei, C. T. Synthesis, structure and fluorescence analysis of three Zn(II) complexes based on (1-methyl-1H-benzimidazol-2-yl) methanol. *Chin. J. Inorg. Chem.* **2023**, *39* (9), 1782−1790.
(24) Li, M.; Zhang, Z.; Yu, Y.; Yuan, H.; Nezamzadeh-Ejhieh, A.; Liu, J.; Pan, Y.; Lan, Q. Recent advances in Zn-MOFs and their derivatives for cancer therapeutic applications. *Mater. Adv.* **2023**, *4* (21), 5050−5093.
(25) Sun, H.; Chen, S.; Zhong, A.; Sun, R.; Jia, J.; Yang, J.; Liu, D.; Niu, J.; Lu, S. Tuning photophysical properties via positional isomerization of the pyridine ring in donor−acceptor-structured aggregation-induced emission luminogens based on phenylmethylene pyridineacetonitrile derivatives. *Molecules* **2023**, *28* (7), 3282.
(26) Zhong, Y.; Peng, Z.; Peng, Y.; Li, B.; Pan, Y.; Ouyang, Q.; Sakiyama, H.; Muddassir, M.; Liu, J. Construction of Fe-doped ZIF-8/DOX nanocomposites for ferroptosis strategy in the treatment of breast cancer. *J. Mater. Chem. B* **2023**, *11* (27), 6335−6345.
(27) Chen, X.; Li, M.; Lin, M.; Lu, C.; Kumar, A.; Pan, Y.; Liu, J.; Peng, Y. Current and promising applications of Hf (IV)-based MOFs in clinical cancer therapy. *J. Mater. Chem. B* **2023**, *11* (25), 5693−5714.
(28) Huang, P.; Yao, L.; Chang, Q.; Sha, Y.; Jiang, G.; Zhang, S.; Li, Z. Room-temperature preparation of highly efficient NH_2-MIL-101(Fe) catalyst: The important role of−NH_2 in accelerating Fe(III)/Fe(II) cycling. *Chemosphere* **2022**, *291*, No. 133026.
(29) Vitillo, J. G.; Lu, C. C.; Cramer, C. J.; Bhan, A.; Gagliardi, L. Influence of first and second coordination environment on structural Fe(II) sites in MIL-101 for C−H bond activation in methane. *ACS Catal.* **2021**, *11* (2), 579−589.
(30) Huang, P.; Chang, Q.; Jiang, G.; Cao, K.; Wang, X. MIL-101 (FeII3, Mn) with dual-reaction center as Fenton-like catalyst for highly efficient peroxide activation and phenol degradation. *Sep. Purif. Technol.* **2023**, *306*, No. 122582.
(31) Som, I.; Roy, M.; Saha, R. Advances in Nanomaterial-based Water Treatment Approaches for Photocatalytic Degradation of Water Pollutants. *ChemCatChem.* **2020**, *12* (13), 3409−3433.
(32) Taha, A. A.; Huang, L.; Ramakrishna, S.; Liu, Y. MOF [NH_2-MIL-101 (Fe)] as a powerful and reusable Fenton-like catalyst. *J. Water Process Eng.* **2020**, *33*, No. 101004.
(33) Vu, T. A.; Le, G. H.; Dao, C. D.; Dang, L. Q.; Nguyen, K. T.; Dang, P. T.; Tran, H. T. K.; Duong, Q. T.; Nguyen, T. V.; Lee, G. D. Isomorphous substitution of Cr by Fe in MIL-101 framework and its application as a novel heterogeneous photo-Fenton catalyst for reactive dye degradation. *RSC Adv.* **2014**, *4* (78), 41185−41194.
(34) Liu, Y. H.; Lv, J. A.; Xu, M. M.; Dong, C.; Liu, X. M.; Li, J. R.; Xie, L. H. Birnessite-type manganese dioxide nanosheets on metal−organic frameworks with high catalytic activity in ozone decomposition. *ACS Appl. Nano Mater.* **2023**, *6* (9), 7794−7801.
(35) Dong, C.; Yang, J. J.; Xie, L. H.; Cui, G.; Fang, W. H.; Li, J. R. Catalytic ozone decomposition and adsorptive VOCs removal in bimetallic metal-organic frameworks. *Nat. Commun.* **2022**, *13* (1), 4991.
(36) Balachandran, V.; Karunakaran, V. Quantum mechanical study of the structure and vibrational spectroscopic (FT-IR and FT-Raman), first-order hyperpolarizability, NBO and HOMO-LUMO studies of 4-bromo-3-nitroanisole. *Spectrochim. Acta, Part A* **2013**, *106*, 284−298.
(37) Variava, M. F.; Church, T. L.; Harris, A. T. Magnetically recoverable Fe_xO_y−MWNT Fenton's catalysts that show enhanced activity at neutral pH. *Appl. Catal. B - Environ.* **2012**, *123*, 200−207.
(38) Nasirian, M.; Mehrvar, M. Photocatalytic degradation of aqueous Methyl Orange using nitrogen-doped TiO_2 photocatalyst prepared by novel method of ultraviolet-assisted thermal synthesis. *J. Environ. Sci.* **2018**, *66*, 81−93.
(39) Zhou, F.; Yan, C.; Liang, T.; Sun, Q.; Wang, H. Photocatalytic degradation of Orange G using sepiolite-TiO_2 nanocomposites: Optimization of physicochemical parameters and kinetics studies. *Chem. Eng. Sci.* **2018**, *183*, 231−239.
(40) Fattahi, M.; Niaz, Z.; Esmaeili, F.; Mohammadi, A. A.; Shams, M.; Nguyen Le, B. Boosting the adsorptive and photocatalytic performance of MIL-101(Fe) against methylene blue dye through a thermal post-synthesis modification. *Sci. Rep.* **2023**, *13* (1), 14502.
(41) Liu, Y.; Ye, Y.; Dai, M.; Gong, Q.; Dang, Z. Ag/AgCl/MIL-101(Fe) catalyzed degradation of methylene blue under visible light irradation. *Materials* **2019**, *12* (9), 1453.
(42) Thanh, H. T. M.; Tu, N. T. T.; Hung, N. P.; Tuyen, T. N.; Mau, T. X.; Khieu, D. Q. Magnetic iron oxide modified MIL-101 composite as an efficient visible-light-driven photocatalyst for methylene blue degradation. *J. Porous Mater.* **2019**, *26* (6), 1699−1712.
(43) Yang, S.; Chen, Y.; Li, S.; Chen, H. Efficient photocatalytic performance and the mechanism of copper (i) metal−organic framework nanosheets. *New J. Chem.* **2023**, *47* (32), 15348−15356.

https://doi.org/10.1021/acsomega.4c03616
ACS Omega 2024, 9, 32864−32872